Steel and Composite Structures, Vol. 12, No. 6 (2012) 491-504
DOI: http://dx.doi.org/10.12989/scs.2012.12.6.491

Nonlinear cylindrical bending of functionally graded carbon nanotube-reinforced composite plates

Abdelhakim Kaci, Abdelouahed Tounsi*, Karima Bakhti and El Abbas Adda Bedia

Laboratoire des Matériaux et Hydrologie, Université de Sidi Bel Abbes, Algérie

(Received July 01, 2011, Revised March 15, 2012, Accepted March 30, 2012)

Abstract. In this paper, the nonlinear cylindrical bending of simply supported, functionally graded nanocomposite plates reinforced by single-walled carbon nanotubes (SWCNTs), is studied. The plates are subjected to uniform pressure loading in thermal environments and their geometric nonlinearity is introduced in the strain–displacement equations based on Von-Karman assumptions. The material properties of SWCNTs are assumed to be temperature-dependent and are obtained from molecular dynamics simulations. The material properties of functionally graded carbon nanotube-reinforced composites (FG-CNTCRs) are assumed to be graded in the thickness direction, and are estimated through a micromechanical model. The governing equations are reduced to linear differential equation with nonlinear boundary conditions yielding a simple solution procedure. Numerical results are presented to show the effect of the material distribution on the deflections and stresses.

Keywords: plate; nano-composites; analytical modeling; functionally graded materials.

1. introduction

The exceptional mechanical, thermal and electrical properties of carbon nanotubes (CNTs) show significant promises as a potential reinforcing phase and multifunctional element in polymer matrix composites (PMC) (Iijima 1991, Lu 1997, Treacy *et al.* 1996, Wong *et al.* 1997, Wagner *et al.* 1998, Lourie and Wagner 1998, Lourie *et al.* 1998, Yakobson *et al.* 1996, Thostenson *et al.* 2001, Sandler *et al.* 1999, Ajayan *et al.* 2000, Lake *et al.* 2002, Lau and Hui 2002). The most important features of carbon nanotubes are their extremely high stiffness combined with excellent resilience. For example, it has been reported that carbon nanotubes possess very high elastic modulus and sustain large elastic strain up to 5% (Qian *et al.* 2000). Therefore, the introduction of carbon nanotubes into polymers may improve their applications in the fields of reinforcing composites, electronic devices and more.

Most studies on carbon nanotube-reinforced composites (CNTRCs) have focused on their material properties (Odegard *et al.* 2003, Hu *et al.* 2005, Fidelus *et al.* 2005, Bonnet *et al.* 2007, Han and Elliott 2007, Zhu *et al.* 2007). Several investigations have shown that the addition of small amounts of carbon nanotube can considerably improve the mechanical, electrical and thermal properties of polymeric composites (Fidelus *et al.* 2005, Bonnet *et al.* 2007, Han and Elliott 2007, Zhu *et al.* 2007). Even though these studies are quite useful in establishing the stress- strain behavior of the nanocomposites,

* Corresponding author, Professor, E-mail: tou_abdel@yahoo.com

their use in actual structural applications is the ultimate purpose for the development of this advanced class of materials. As a result, there is a need to observe the global response of CNTRCs in an actual structural element. Wuite and Adali (2005) presented a multi-scale analysis of the deflection and stress behavior of CNT reinforced polymer composite beams. The micromechanics models used in the study include straight CNTs aligned in one direction, randomly oriented CNTs and a two parameter model of agglomeration. Vodenitcharova and Zhang (2006) studied the pure bending and bending-induced local buckling of a nanocomposite beam reinforced by a singlewalled carbon nanotube. Recently, Salehi-Khojin and Jalili (2008) considered the buckling of boron nitride nanotube reinforced piezoelectric polymeric composites subjected to combined electrothermo-mechanical loadings. Ray and Batra (2007) proposed a new 1-3 piezoelectric composite comprised of armchair SWCNTs embedded in a piezoceramic matrix for the active control of smart structures.

It is well-known that the applications of CNTs to nanocomposites have been hindered due to the weak interfacial bonding between CNTs and matrix. Functionally graded materials (FGMs) are inhomogeneous composites characterized by smooth and continuous variations in both compositional profile and material properties and have found a wide range of applications in many industries (Suresh and Mortensen 1998). The static bending, elastic buckling, postbuckling, linear and nonlinear free vibration of FGM structures have been extensively investigated (Benatta *et al.* 2008, Sallai *et al.* 2009, Şişmek and Kocaturk 2009, Şişmek 2010a, 2010b, 2010c, Na and Kim 2009, Wu *et al.* 2007, Ke *et al.* 2009). By using the concept of FGM, Shen (2009) suggested that the interfacial bonding strength can be improved through the use of a graded distribution of CNTs in the matrix and examined the nonlinear bending behavior of simply supported, functionally graded nanocomposite plates reinforced by SWCNTs subjected to a transverse uniform or sinusoidal load in thermal environments. Based on Timoshenko beam theory and von Karman geometric nonlinearity, Ke *et al.* (2010) investigated the nonlinear free vibration of functionally graded nanocomposite beams reinforced by single-walled carbon nanotubes (SWCNTs).

In this study, a nonlinear cylindrical bending behavior of functionally graded nanocomposite plates reinforced by the SWCNT is studied. The material properties of the FG-CNTRC are assumed to be graded in the thickness direction and estimated though the rule of mixture in which the CNT efficiency parameter is determined by matching the elastic modulus of CNTRCs obtained from MD simulation with the numerical results calculated from the rule of mixture. The Classical Plate Theory (CPT) and the von Karman-type nonlinear strains are used to construct the problem governing equations. Numerical results are presented to show the influence of material properties, plate geometry and mechanical loading on the resulting transverse deflection and stress state.

2. Material properties of functionally graded CNTRC plates

Fig. 1 shows the CNTRCs of thickness h where the distribution of CNTs is uniform across the thickness direction in Fig. 1(a) (UD-CNTRC) and is non-uniform and graded along the thickness direction in Fig. 1(b) (FG-CNTRC), respectively. It is assumed that the CNTRC is made from a mixture of SWCNT and an isotropic matrix. We first determine the effective material properties of CNTRC. It was pointed out by Han and Elliott (2007) that the material properties of the SWCNT and CNTRC are anisotropic. According to the rule of mixture, the effective Young's modulus, the shear modulus and the thermal expansion coefficient of CNTRC can be expressed as (Shen 2009)

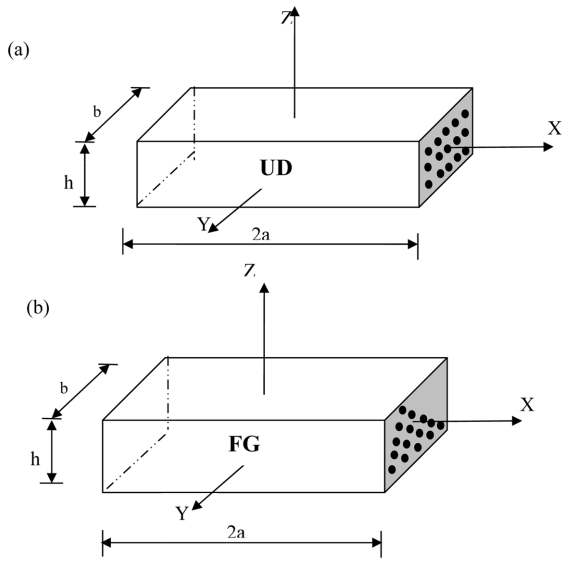

Fig. 1 Geometry of carbon nanotube-reinforced composites: (a) UD-CNTRC and (b) FG-CNTRC

$$E_{11} = \eta_1 V_{CN} E_{11}^{CN} + V_m E^m \tag{1a}$$

$$\frac{\eta_2}{E_{22}} = \frac{V_{CN}}{E_{22}^{CN}} + \frac{V_m}{E^m} \tag{1b}$$

$$\frac{\eta_3}{G_{12}} = \frac{V_{CN}}{G_{12}^{CN}} + \frac{V_m}{G^m} \tag{1c}$$

$$\alpha_{11} = V_{CN}\alpha_{11}^{CN} + V_m\alpha^m \tag{1d}$$

$$\alpha_{22} = (1+\nu_{12}^{CN})V_{CN}\alpha_{22}^{CN} + (1+\nu^m)V_m\alpha^m - \nu_{12}\alpha_{11} \tag{1e}$$

where E_{11}^{CN}, E_{22}^{CN}, G_{12}^{CN}, α_{11}^{CN} and α_{22}^{CN} are the Young's modulus, shear modulus and thermal expansion coefficient, respectively, of the carbon nanotube, and E^m, G^m and α^m are corresponding properties for the matrix. ν_{12}^{CN} and ν^m are Poisson's ratios, respectively, of the carbon nanotube and matrix. To account for the scale-dependent material properties Eq. (1) includes η_j (j = 1, 2, 3) which is called the CNT efficiency parameter, and will be determined later by matching the elastic modulus of CNTRCs observed from the MD simulation results with the numerical results obtained from the rule of mixture. V_{cn} and V_m are the carbon nanotube and matrix volume fractions and are related by

$$V_{CN} + V_m = 1 \tag{2a}$$

We assume the volume fraction V_{cn} follows as:

$$V_{CN} = \left(1 - \frac{2z}{h}\right) V_{CN}^* \tag{2b}$$

in which

$$V_{CN}^{*} = \frac{W_{CN}}{W_{CN} + (\rho_{CN}/\rho_m) - (\rho_{CN}/\rho_m) W_{CN}} \tag{2c}$$

where W_{CN} is the mass fraction of nanotube, and ρ_{CN} and ρ_m are the densities of carbon nanotube and matrix, respectively. In such a way, the two cases of uniformly distributed (UD), i.e. $V_{CN} = V_{CN}^{*}$, and functionally graded (FG) CNTRCs will have the same value of mass fraction of nanotube.

The Poisson's ratio is assumed to be uniformly distributed, i.e.

$$\nu_{12} = V_{CN}^{*} \nu_{12}^{CN} + V_m \nu^m \tag{2d}$$

3. Governing equations for nonlinear bending of FG-CNTRC plates

The fundamental equations of large deflection analysis of pressure loaded FG-CNTRC plates are briefly outlined in this section. Based on Kirchhoff's hypotheses and von Karman large deflection theory, the strain-displacement relations may be written as

$$\begin{aligned} \varepsilon_x &= \varepsilon_x^0 + z k_x, \qquad & \varepsilon_y &= \varepsilon_y^0 + z k_y \\ \gamma_{xy} &= \gamma_{xy}^0 + z k_{xy}, \qquad & \varepsilon_z &= \gamma_{yz} = \gamma_{xz} = 0 \end{aligned} \tag{3}$$

where

$$\begin{aligned} \varepsilon_x^0 &= u_{,x} + \frac{1}{2} w_{,x}^2, \qquad & \varepsilon_y^0 &= v_{,y} + \frac{1}{2} w_{,x}^2 \\ \gamma_{xy}^0 &= u_{,y} + v_{,x} + w_{,x} w_{,y} \\ k_x &= -w_{,xx}, \; k_y = -w_{,yy} \qquad \text{and} \qquad k_{xy} = -2 w_{,xy} \end{aligned} \tag{4}$$

where (u, v, w) are the mid-displacements in the (x, y, z) directions, respectively. Also, $(\varepsilon_x^0, \varepsilon_y^0, \gamma_{xy}^0)$ and (k_x, k_y, k_{xy}) are the mid-plane strains and mid-plane curvatures. The subscript commas represent differentiation.

The constitutive relations for nonzero strains are given by

$$\begin{Bmatrix} \sigma_x \\ \sigma_y \\ \tau_{xy} \end{Bmatrix} = \begin{bmatrix} Q_{11} & Q_{12} & 0 \\ Q_{12} & Q_{22} & 0 \\ 0 & 0 & Q_{66} \end{bmatrix} \cdot \begin{Bmatrix} \varepsilon_x - \alpha_{11} \Delta T \\ \varepsilon_y - \alpha_{22} \Delta T \\ \gamma_{xy} \end{Bmatrix} \tag{5}$$

where $\Delta T = T - T_0$ is temperature rise from some reference temperature T_0 at which there are no thermal strains.

Using the material properties defined in Eq. (1), the stiffness coefficients, Q_{ij}, can be expressed as

$$Q_{11} = \frac{E_{11}}{1 - \nu_{12}\nu_{21}}, \; Q_{22} = \frac{E_{22}}{1 - \nu_{12}\nu_{21}}, \; Q_{12} = \frac{\nu_{12} E_{11}}{1 - \nu_{12}\nu_{21}}, \; Q_{66} = G_{12} \tag{6}$$

where E_{11}, E_{22}, G_{12}, ν_{12} and ν_{21} have their usual meanings, in particular for an CNTRC layer they are

given in detail in Eqs. (1) and (2).

Using Eq. (5) in conjunction with the strain components in Eq. (3), the constitutive relation for the CNTRC plate may be written as

$$\begin{Bmatrix} N \\ M \end{Bmatrix} = \begin{bmatrix} A & B \\ B & D \end{bmatrix} \begin{Bmatrix} \varepsilon^0 \\ k \end{Bmatrix} - \begin{Bmatrix} N^T \\ M^T \end{Bmatrix} \tag{7}$$

where A, B and D are the (3×3) matrices given by

$$(A_{ij}, B_{ij}, D_{ij}) = \int_{-h/2}^{h/2} \sigma_i(1, z, z^2)dz \tag{8}$$

N and M are (3×3) matrices of the resultants normal forces and bending moments, respectively, defined in the usual manner, i.e.,

$$(N_i, M_i) = \int_{-h/2}^{h/2} \sigma_i(1, z)dz \tag{9}$$

The equivalent thermal loads (N^T and M^T) are defined by the relations

$$(N^T, M^T) = \int_{-h/2}^{h/2} Q_{ij}\alpha_j \Delta T(1, z)dz \tag{10}$$

Use of Hamilton's principle yields the Euler–Lagrange equations as (Reddy 2003)

$$N_{x,x} + N_{xy,y} = 0 \tag{11a}$$

$$N_{xy,x} + N_{y,y} = 0 \tag{11b}$$

$$M_{x,xx} + 2M_{xy,xy} + M_{y,yy} + N_x w_{,xx} + 2N_{xy} w_{,xy} + N_y w_{,yy} + q = 0 \tag{11c}$$

where q is the transverse loading on the plate.

4. Cylindrical bending

In the case of cylindrical bending, the plate deformation is assumed to be independent of one of the axes in the plane of the plate. If this axis is chosen as y, the displacements are expressed as

$$u = u(x), \; v = 0 \quad \text{and} \quad w = w(x) \tag{12}$$

Thus, the plate remains in the state of plane-strain in the x-z plane. In view of displacements given by Eq. (12), the plate equilibrium Eq. (11) simplifies to

$$N_{x,x} = 0 \tag{13}$$

and

$$M_{x,xx} + N_x \cdot w_{,xx} + q = 0 \tag{14}$$

Eq. (13) leads to

$$N_x = \text{constant} = N_x^0 \tag{15}$$

Therefore, Eq. (14) becomes

$$M_{x,xx} + N_x^0 \cdot w_{,xx} + q = 0 \tag{16}$$

From Eq. (7)

$$\{N\} = [A]\{\varepsilon^0\} + [B]\{k\} - \{N^T\} \tag{17a}$$

$$\{M\} = [B]\{\varepsilon^0\} + [D]\{k\} - \{M^T\} \tag{17b}$$

For the case of cylindrical bending

$$N_x = A_{11}\varepsilon_x^0 + B_{11}k_x - N_x^T \tag{18a}$$

$$M_x = B_{11}\varepsilon_x^0 + D_{11}k_x - M_x^T \tag{18b}$$

Now, substitution of ε_x^0 and k_x values from Eq. (4) gives

$$N_x = N_x^0 = A_{11}\left(u_{,x} + \frac{1}{2}w_{,x}^2\right) - B_{11}w_{,xx} - N_x^T \tag{19a}$$

$$M_x = B_{11}\left(u_{,x} + \frac{1}{2}w_{,x}^2\right) - D_{11}w_{,xx} - M_x^T \tag{19b}$$

Eq. (19) yield

$$M_x = \frac{B_{11}}{A_{11}}(N_x^0 + N_x^T) + \left(\frac{B_{11}^2}{A_{11}} - D_{11}\right)w_{,xx} - M_x^T \tag{20}$$

Plugging in this value of M_x in Eq. (14), gives

$$\left(\frac{B_{11}^2}{A_{11}} - D_{11}\right)w_{,xxxx} + N_x^0 w_{,xx} + q = 0 \tag{21}$$

which can be put in the form

$$w_{,xxxx} - p^2 w_{,xx} = q_0 \tag{22}$$

where

$$p^2 = \frac{N_x^0}{(D_{11} - B_{11}^2/A_{11})} \quad \text{and} \quad q_0 = \frac{q}{(D_{11} - B_{11}^2/A_{11})} \tag{23}$$

5. General solution

In this study it is assumed that an FG-CNTRC plate is subjected to a uniform transverse load q on its top surface. It is intended here to obtain analytical solutions for the non-linear bending of the FG-CNTRC plate.

5.1 Nonlinear analysis

Eq. (22) is a linear fourth-order ordinary differential equation whose solution is readily available. The general solution is as follows

$$w(x) = C_1 cosh(px) + C_2 - \frac{q_0}{2p^2}x^2 \tag{24}$$

where C_1 and C_2 are constants, which must be determined using BCs at either edges of the plate. Assume that the origin of the coordinate system is located at the plate mid-span; accordingly, the simply supported BCs yield

$$w(\pm a) = 0,\ M_x(\pm a) = 0 \quad \text{and} \quad u(\pm a) = 0 \tag{25}$$

Using Eq.(24) in Eq.(20)

$$M_x = \frac{B_{11}}{A_{11}}(N_x^0 + N_x^T) + \left(\frac{B_{11}^2}{A_{11}} - D_{11}\right)\left(C_1 p^2 cosh(px) - \frac{q_0}{p^2}\right) - M_x^T \tag{26}$$

which, on applying the boundary condition $M_x(\pm a) = 0$, gives

$$C_1 = \frac{1}{cosh(pa)}\left\{\frac{1}{N_x^0}\left(\frac{B_{11}}{A_{11}}N_x^T - M_x^T\right) + \frac{B_{11}}{A_{11}} + \frac{q_0}{p^4}\right\} \tag{27}$$

The boundary condition $w(\pm a) = 0$ gives

$$C_2 = \frac{q_0 a^2}{2p^2} - C_1 cosh(pa) \tag{28}$$

Integrating of Eq.(19a) with respect to x, and application of the boundary condition $u(\pm a) = 0$ leads to

$$\frac{N_x^0 + N_x^T}{A_{11}} + \frac{B_{11}}{A_{11}} p C_1 sinh(pa) - \frac{B_{11}}{A_{11}}\frac{q_0 a}{p^2} - \frac{q_0^2 a^3}{6p^4} + \frac{p^2 C_1^2 a}{4}$$

$$-\frac{pC_1^2}{8}sinh(2pa) + \frac{C_1 q_0}{p^3}[Pacosh(pa) - sinh(pa)] = 0 \tag{29}$$

Eqs. (27)-(29) contain three unknowns quantities: C_1, C_2 and N_x^0 and a numerical technique must be used to obtain a solution.

If N_x^0 is negative, the solution of Eq. (22) becomes

$$w(x) = C_1 cos(px) + C_2 + \frac{q_0 x^2}{2p^2} \tag{30}$$

which on applying the boundary conditions of Eq.(25), gives

$$C_1 = \frac{1}{cos(pa)}\left\{\frac{1}{N_x^0}\left(\frac{B_{11}}{A_{11}}N_x^T - M_x^T\right) + \frac{B_{11}}{A_{11}} + \frac{q_0}{p^4}\right\} \tag{31}$$

$$C_2 = \frac{-q_0 a^2}{2p^2} - C_1 cos(pa) \tag{32}$$

and

$$\frac{N_x^0 + N_x^T}{A_{11}}a - \frac{B_{11}}{A_{11}}pC_1 sin(pa) + \frac{B_{11}}{A_{11}}\frac{q_0 a}{p^2} - \frac{q_0^2 a^3}{6p^4} - \frac{p^2 C_1^2 a}{4}$$

$$+\frac{pC_1^2}{8}sin(2pa) + \frac{C_1 q_0}{p^3}[-pacos(pa) + sin(pa)] = 0 \tag{33}$$

Again, Eq. (33) is a transcendental equation and Eqs. (31)-(33) are to be solved numerically.

5.2 Linear analysis

The displacement equations according to classical linear theory can be obtained by setting $p = 0$ in Eq. (22). The following solution for the linear analysis is obtained

$$w(x) = \frac{q_0}{24}(x^4 - a^4) - \left(\frac{3D_{11}A_{11} - 2B_{11}^2}{12D_{11}A_{11}}\right)q_0 a^2(x^2 - a^2) - \frac{M_x^T}{2D_{11}}(x^2 - a^2) \tag{34a}$$

$$u(x) = \frac{B_{11}}{6A_{11}}q_0 x(x^2 - a^2) \tag{34b}$$

6. Numerical results and discussion

Numerical results are presented in this section for FG-CNTRC plates subjected to a transverse uniform load. We first need to determine the effective material properties of CNTRCs. Poly{(*m-phenylenevinylene*)-co-[(*2.5-dioctoxy-p-phenylene*)*vinylene*]}, referred to as PmPV, is selected for the matrix, and the material properties of which are assumed to be $\nu^m = 0.34$, $\alpha^m = 45(1 + 0.0005\Delta T) \times 10^{-6}$/K and $E^m = (3.51 - 0.0047T)$ GPa, in which $T = T_0 + \Delta T$ and $T_0 = 300$ K (room temperature). In such a way, $\alpha^m = 45.0 \times 10^{-6}$ /K and $E^m = 2.1$ GPa at $T_0 = 300$ K. (10, 10) SWCNTs are selected as reinforcements. It has been shown (Elliott *et al.* 2004, Jin and Yuan 2003, Chang *et al.* 2005) the material properties of SWCNTs are anisotropic, chirality-and size-dependent and temperature-dependent. Therefore, all effective elastic properties of a SWCNT need to be carefully determined, otherwise the results may be incorrect.

From MD simulation results the size-dependent and temperature-dependent material properties for armchair (10, 10) SWCNT can be obtained numerically (Shen 2009). Typical results are listed in Table 1. It is noted that the effective wall thickness obtained for (10, 10) - tube is $h = 0.067$ nm, and the wide used value of 0.34 nm for tube wall thickness is thoroughly inappropriate to SWCNTs.

The key issue for successful application of the rule of mixture to CNTRCs is to determine the CNT

Table 1 Temperature-dependent material properties for (10, 10) SWCNT (L = 9.26 nm, R = 0.68 nm, h = 0.067 nm, v_{12}^{CN} = 0.175)

Temperature (K)	E_{11}^{CN} (TPa)	E_{22}^{CN} (TPa)	α_{11}^{CN} (× 10^{-6} /K)
300	5.6466	7.0800	3.4584
500	5.5308	6.9348	4.5361
700	5.4744	6.8641	4.6677

Table 2 Comparisons of Young's moduli for PmPV/CNT composites reinforced by (10,10)-tube under T = 300 K

V_{cn}^{*}	MD (Han and Elliott, 2007)	Rule of mixture	
	E_{11} (GPa)	E_{11} (GPa)	η_1
0.11	94.8	94.57	0.149
0.14	120.2	120.09	0.150
0.17	145.6	145.08	0.149

efficiency parameter η_1. For short fiber composites η_1 is usually taken to be 0.2 (Fukuda and Kawata, 1974). However, there are no experiments conducted to determine the value of η_1 for CNTRCs. Recently, Shen (2009) gives an estimation of CNT efficiency parameter η_1 by matching the Young's moduli E_{11} of CNTRCs obtained by the rule of mixture to those from the MD simulations given by Han and Elliott (2007). Through comparison, we find that the Young's moduli obtained from the rule of mixture and MD simulations can match very well if the CNT efficiency parameter η_1 is properly chosen, as shown in Table 2.

The plate geometry is chosen so the h = 5 mm and α = 0.5 m. The results obtained from the analysis are presented in dimensionless parametric terms of deflections and stresses as follows:

side coordinate $\bar{x} = x/a$
thickness coordinate $\bar{z} = z/h$

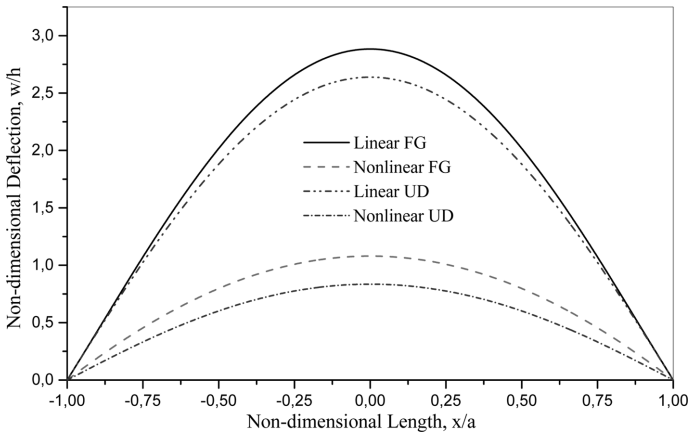

Fig. 2 Non-dimensional deflections of CNTRC plate subjected to a uniform transverse load q = 1 KN/m^2 versus non-dimensional length for V_{CN}^{*} = 0.11, T = 300 K

deflection $\overline{w} = w/h$
axial stress $\bar{\sigma}_x = \sigma_x h^2/[(q + 10^{-6} E_{22}^{CN} \alpha_{22}^{CN} \Delta T)a^2]$
load parameter $q^n = qa^4/(E_{22}^{CN} h^4)$

The CNTRC plate is subjected to a transverse load of $q = 1$ KN/m^2 as an example. The non-dimensional deflection is shown in Fig. 2 under thermal environmental condition $T = 300$ K. A same size uniformly distributed CNTRC plate is also considered as a comparator. In this figure, UD represents uniformly distributed CNTRC plate and FG represents functionally graded CNTRC plate. It can be seen that the linear solution overestimates the deflections of both FG- and UD- CNTRC plates and the deflections of FG-CNTRC plate are larger than that of the UD-CNTRC plate.

Fig. 3 presents the effect of nanotube volume fraction on the non-dimensional deflection of CNTRC plates for different values of the nanotube volume fraction $V_{cn}^* = (0.11, 0.14, 0.17)$ subjected to a uniform pressure under thermal environmental condition $T = 300$ K in non-linear analysis. It can be

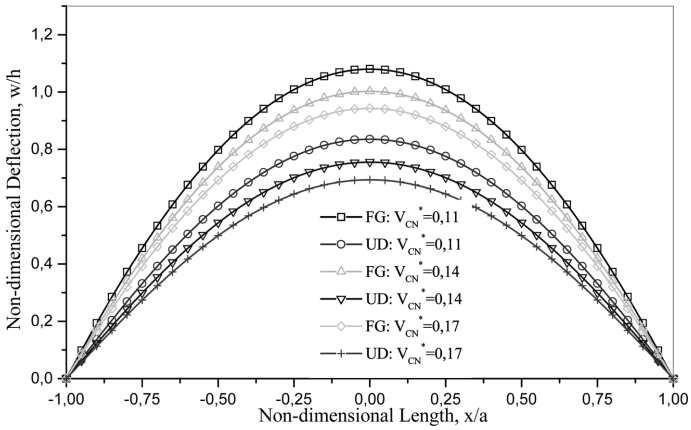

Fig. 3 Effects of nanotube volume fraction on the nonlinear bending behavior of CNTRC plates under uniform pressure $q = 1$ KN/m^2 and $T = 300$ K

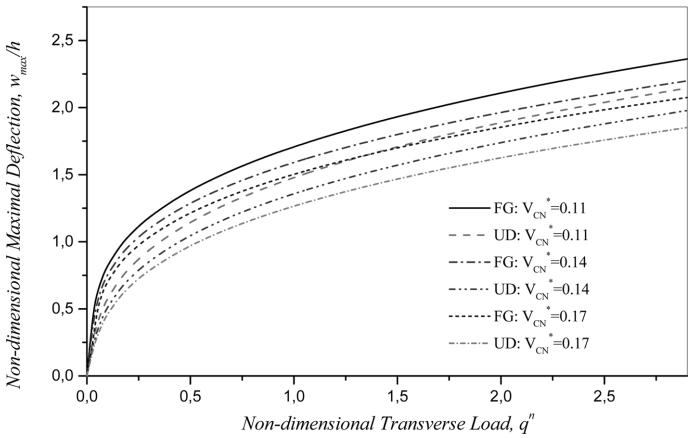

Fig. 4 Variation of the non-dimensional center deflection w_{max} of the CNTRC plate versus q^n for various volume fraction V_{CN}^*

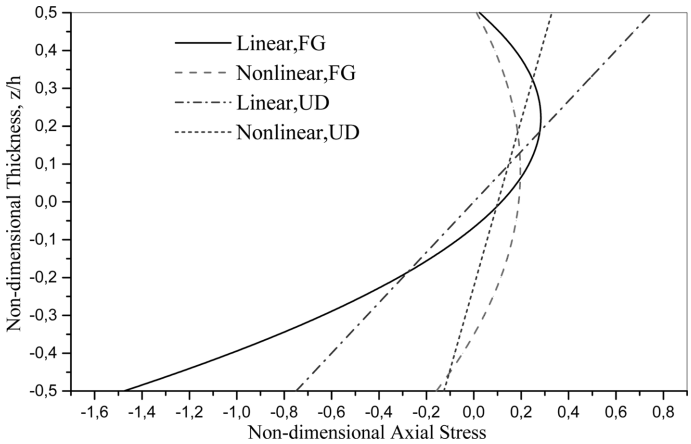

Fig. 5 Through the thickness distribution of the mid-span non-dimensional axial stress $\bar{\sigma}_x$ of the CNTRC plate subjected to $q = 1$ KN/m^2 for $V_{CN}^* = 0.11$ and $T = 300$ K

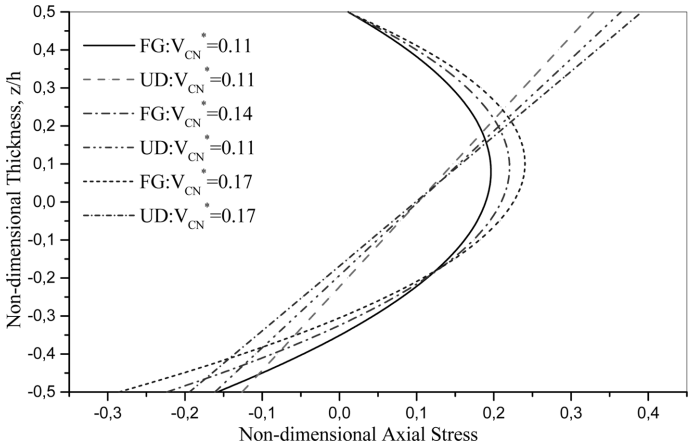

Fig. 6 Effects of nanotube volume fraction on the mid-span non-dimensional axial stress $\bar{\sigma}_x$ of the CNTRC plate subjected to $q = 1$ KN/m^2 and $T = 300$ K

seen that the plate has higher deflection when it has lower volume fraction. It can be also found that deflections of FG-CNTRC plate are larger than those of the UD-CNTRC plate.

Fig. 4 presents the load-deflection curves for FG- and UD- CNTRC square plates with different values of the nanotube volume fraction $V_{cn}^* = (0.11, 0.14, 0.17)$ subjected to a uniform pressure under thermal environmental condition $T = 300$ K in non-linear analysis. It can be found that the central deflection of FG-CNTRC plate is larger than that of the UD-CNTRC plate, and the difference becomes larger when the transverse pressure is sufficiently large. It can be also seen that the plate has higher deflection when it has lower volume fraction.

Fig. 5 shows through the thickness distributions of the non-dimensional axial stress $\bar{\sigma}_x$ of CNTRC plate subjected to $q = 1$ KN/m^2 under thermal environmental condition $T = 300$ K. Under the application of the pressure loading, the stresses are compressive at the bottom surface and tensile at the top surface. In the case of linear analysis, it can be seen that for a UD-CNTRC plate, the magnitude of

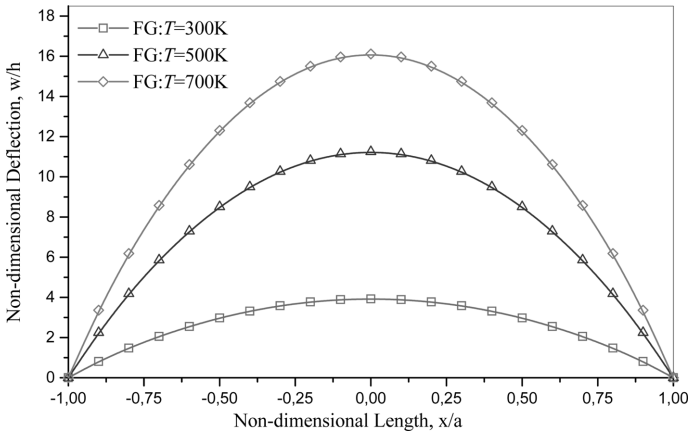

Fig. 7 Effects of temperature changes on the nonlinear bending behavior of CNTRC plates under uniform pressure $q = 100$ KN/m^2 for $V_{CN}^{*} = 0.17$

the tensile and compressive stresses are equal and located at the top and bottom surfaces. However, in the case of non-linear analysis, this remark is not checked. The stress profile for UD-CNTRC plate changes linearly through the thickness for both linear and non-linear solutions.

Fig. 6 shows the effect of nanotube volume fraction on the non-dimensional axial stress $\bar{\sigma}_x$ through the thickness of CNTRC plates for different values of the nanotube volume fraction $V_{cn}^{*} = (0.11, 0.14, 0.17)$ subjected to a uniform pressure under thermal environmental condition $T = 300$ K in non-linear analysis. It can be seen that the non-dimensional axial stress $\bar{\sigma}_x$ increases with the volume fraction

Fig. 7 presents non-dimensional deflection of CNTRC plates subjected to a uniform pressure and under three sets of thermal environmental conditions $T = 300$; 500 and 700 K using non-linear analysis. Since the material properties for both matrix and SWCNTs are assumed to be temperature-dependent, the variation of temperature reduces the elastic moduli and degrades the strength of the nanocomposites. It can be seen that the deflections are increased with increases in temperature.

7. Conclusions

The nonlinear cylindrical bending of functionally graded carbon nanotube-reinforced composite plates subjected to transverse loads is studied using a simple analytical solution. The material properties of FG-CNTRC are assumed to be graded in the thickness and estimated though the rule of mixture. Navier equations according to the large deflection theory can be expressed as linear equations for the deflection, leaving nonlinear boundary conditions. This linearity of the differential equations greatly simplifies the large deflection analysis. From this study it is concluded that because of extension-bending coupling, the large deflection plate theory must be used even for deflection that are normally considered small. In comparison with the nonlinear analysis, the linear solution overestimates. The results show also that the plate has higher deflection when it has lower volume fraction and the deflections of FG-CNTRC plate are larger than those of the UD-CNTRC plate.

Acknowledgments

This research was supported by the Algerian national agency for development of university research (ANDRU) and university of Sidi Bel Abbes (UDL SBA) in Algeria.

References

Ajayan, P.M., Schadler, L.S., Giannaris, C. and Rubio, A. (2000), "Single-walled carbon nanotube polymer composites: strength and weakness," *Adv. Mater.*, **12**, 750-753.

Benatta, M.A., Mechab, I., Tounsi, A. and Adda bedia, E.A. (2008), "Static analysis of functionally graded short beams including warping and shear deformation effects," *Comput. Materials Sci.*, **44**(2), 675-776.

Bonnet, P., Sireude, D., Garnier, B. and Chauvet, O. (2007), "Thermal properties and percolation in carbon nanotube–polymer composites," *J. Appl. Phys*., **91**(20), 201910.

Chang, T., Geng, J. and Guo, X. (2005), "Chirality- and size-dependent elastic properties of single-walled carbon nanotubes," *Appl. Phys. Lett.*, **87**(25), 251929.

Elliott, J.A., Sandler, J.K.W., Windle, A.H., Young, R.J. and Shaffer, M.S.P. (2004), "Collapse of single wall carbon nanotubes is diameter dependent," *Phys. Rev. Lett.*, **92**(9), 095501.

Fidelus, J.D., Wiesel, E., Gojny, F.H., Schulte, K. and Wagner, H.D. (2005), "Thermo-mechanical properties of randomly oriented carbon/epoxy nanocomposites," *Compos. Part A*, **36**(11), 1555-1561.

Fukuda, H. and Kawata, K. (1974), "On Young's modulus of short fibre composites," *Fibre Sci. Technol.*, **7**(3), 207-222.

Han, Y. and Elliott, J. (2007), "Molecular dynamics simulations of the elastic properties of polymer/carbon nanotube composites," *Comput. Mater. Sci.*, **39**(2), 315-323.

Hu, N., Fukunaga, H., Lu, C., Kameyama, M. and Yan, B. (2005), "Prediction of elastic properties of carbon nanotube reinforced composites," *Proce. Royal. Soc. A*, **461**(2058), 1685-1710.

Jin, Y. and Yuan, F.G. (2003), "Simulation of elastic properties of single-walled carbon nanotubes," *Compos. Sci. Technol.*, **63**(11), 1507-1515.

Ke, L.L., Yang, J. and Kitipornchai, S. (2009), "Postbuckling analysis of edge cracked functionally graded Timoshenko beams under end shortening," *Compos. Struct.*, **90**(2), 152-160.

Ke, L.L., Yang, J. and Kitipornchai, S. (2010), "Nonlinear free vibration of functionally graded carbon nanotube-reinforced composite beams," *Compos. Struct.*, **92**(3), 676-683.

Lake, M.L., Glasgow, D.G. and Kwag, C. (2002), "Nanocomposites from Carbon nanofibers," *Proc. Am. Soc. Comp*.,

Lau, K.T. and Hui, D. (2002), "The revolutionary creation of new advanced materialscarbon nanotube composites," *Composites*, *Part B*, **33**(4), 263-277.

Lijima, S. (1991), "Helical microtubules of graphitic carbon," *Nature*, **354**, 56-58.

Lourie, O., Cox, D.M. and Wagner, H.D. (1998), "Buckling and collapse of embedded carbon nanotubes," *Phys. Rev. Lett.*, **81**(8), 1638-1641.

Lourie, O. and Wagner, H.D. (1998), "Evaluation of Young_s modulus of carbon nanotubes by micro-Raman spectroscopy," *J. Mater. Res.*, **13**(9), 2418-2422.

Lu, J.P. (1997), "Elastic properties of single and multilayered nanotubes," *J. Phy. Chem. Solids*, **58**(11), 1649-1652.

Matsunaga, H. (2009), "Free vibration and stability of functionally graded circular cylindrical shells according to a 2D higher-order deformation theory," *Compos, Struct.*, **88**(4), 519-531.

Na, K.S. and Kim, J.H. (2009), "Three-dimensional thermomechanical buckling analysis for functionally graded composite plates," *Compos. Struct.*, **73**(4), 413-422.

Odegard, G.M., Gates, T.S., Wise, K.E., Park, C. and Siochi, E.J. (2003), "Constitutive modelling of nanotube-reinforced polymer composites," *Compos. Sci. Technol.*, **63**(11), 1671-1687.

Qian, D., Dickey, E.C., Andrews, R. and Rantell, T. (2000), "Load transfer and deformation mechanisms in carbon nanotube-polystyrene composites," *Appl. Phys. Lett.*, **76**(20), 2868-2870.

Ray, M.C. and Batra, R.C. (2007), "A single-walled carbon nanotube reinforced 1-3 piezoelectric composite for

active control of smart structures," *Smart. Mater. Struct.*, **16**(5), 1936-1947.
Reddy, J.N. (2003), "Mechanics of laminated composite plates and shells, theory and analysis," *2nd ed. Boca Raton, FL: CRC Press*.
Salehi-Khojin, A. and Jalili, N. (2008), "Buckling of boron nitride nanotube reinforced piezoelectric polymeric composites subject to combined electro-thermomechanical loadings," *Compos. Sci. Technol.*, **68**(6), 1489-1501.
Sallai, B.O., Tounsi, A., Mechab, I., Bachir Bouiadjra, M., Meradjah, M. and Adda Bedia, E.A. (2009), "A theoretical analysis of flexional bending of Al/Al2O3 S-FGM thick beams," *Computational Mater. Sci.*, **44**(4), 1344-1350.
Sandler, J., Shaffer, M.S.P., Prasse, T., Bauhofer, W., Schulte, K. and Windle, A.H. (1999), "Development of a dispersion process for carbon nanotubes in epoxy matrix and resulting electrical properties," *Polymer*, **40**(21), 5967-5971.
Shen, H.S. (2009), "Nonlinear bending of functionally graded carbon nanotube-reinforced composite plates in thermal environments," *Compos. Struct.*, **91**(1), 9-19.
Suresh, S. and Mortensen, A. (1998), "Fundamentals of functionally graded materials: processing and thermomechanical behavior of graded metals and metalceramic composites," *London: IOM Communications Ltd*.
Şimşek, M. and Kocaturk, T. (2009), "Free and forced vibration of a functionally graded beam subjected to a concentrated moving harmonic load," *Compos. Struct*., **90**(4), 465-473.
Şimşek, M. (2010a), "Vibration analysis of a functionally graded beam under a moving mass by using different beam theories," *Compos. Struct*., **92**(4), 904-917.
Şimşek, M. (2010b), "Fundamental frequency analysis of functionally graded beams by using different higher-order beam theories," *Nuclear Engineering and Design*, **240**(4), 697-705.
Şimşek, M. (2010c), "Non-linear vibration analysis of a functionally graded Timoshenko beam under action of a moving harmonic load," *Compos. Struct*., **92**(10), 2532-2546.
Thostenson, E.T., Ren, Z. and Chou, T.W. (2001), "Advanced in the science and technology of carbon nanotubes and their composites: a review," *Comp. Sci. Tech.*, **61**(13), 1899-1912.
Treacy, M.M.J., Ebbesen, T.W. and Gibson, J.M. (1996), "Exceptionally high Young's modulus observed for individual carbon nanotubes," *Nature*, **381**, 678-680.
Vodenitcharova, T. and Zhang, L.C. (2006), "Bending and local buckling of a nanocomposite beam reinforced by a single-walled carbon nanotube," *Int. J. Solids Struct.*, **43**(10), 3006-3024.
Wagner, H.D., Lourie, O., Feldman, Y. and Tenne, R. (1998), "Stress-induced fragmentation of multiwall carbon nanotubes in a polymer matrix," *Appl. Phys. Lett.*, **72**(2), 188-190.
Wong, E.W., Sheehan, P.E. and Lieber, C.M. (1997), "Nanobeam mechanics: elasticity, strength and toughness of nanorods and nanotubes," *Science*, **277**(5334), 1971-1975.
Wu, T.L., Shukla, K.K. and Huang, J.H. (2007), "Post-buckling analysis of functionally graded rectangular plates," *Compos. Struct.*, **81**(1), 1-10.
Wuite, J. and Adali, S. (2005), "Deflection and stress behaviour of nanocomposite reinforced beams using a multiscale analysis," *Compos. Struct.*, **71**(3-4), 388-396.
Yakobson, B.I., Brabec, C.J. and Bernholc, J. (1996), "Nanomechanics of carbon tubes: instabilities beyond linear response," *J. Phys. Rev. Lett.*, **76**(14), 2511-2514.
Zhu, R., Pan, E. and Roy, A.K. (2007), "Molecular dynamics study of the stress–strain behavior of carbon-nanotube reinforced Epon 862 composites," *Mater. Sci. Eng A*, 447(1-2), 51-57.

CC